Generation of a statistical model of the anatomy of human pelvises

Therese Johansson
Jenny Tiliander

2018

LUND
UNIVERSITY

Master's Thesis in
Biomedical Engineering

Faculty of Engineering LTH
Department of Biomedical Engineering

Supervisors
Lorenzo Grassi
Hanna Isaksson

Abstract

Osteoarthritis and osteoporosis are two medical conditions involving the hip which affect the life quality of many people worldwide. These two diseases are diagnosed with 2D imaging by analysis of radiological measures, bone mineral density and joint space. Computed Tomography (CT) can provide 3D images of the hip, but has higher cost and imposes a higher radiation dose to the patient. Another option (which the Biomechanics group in Lund is working on) is to utilize statistical models to construct a 3D model from a 2D image. The Biomechanics group has developed a statistical model of the anatomical variability of the human femur. Adding an equivalent model for the pelvis would then allow to fully represent the hip joint.

In this study, CT scans from 26 male and 21 female patients scheduled for hip replacement surgery were used to create a Statistical Shape Model (SSM) to describe the shape of pelvis. To be able to generate the SSM, the shapes of all bones were defined by identical meshes. A template mesh was created based on one of the available anatomies and it was then registered to each hip bone. The registered bones were then used to create the SSM. The registration method was evaluated by a point-to-surface distance difference. For the SSM, the shape variation and the reconstruction of the hip bones were evaluated for the whole group and for the male and female patient cohorts within the group.

The SSM created during the study was able to represent the shape variation of both male and female bones. Visually, the gender variance was associated to the width and thickness of the bone, corresponding with the known differences of the pelvic bone between the genders. The results indicate that the model can represent the shape of the bone accurately, independent of gender.

Combined with a statistical model for the femur, the SSM created in this study can be used to provide a 2D to 3D reconstruction of the hip from clinical diagnostic images.

Acknowledgements

This master's thesis has been performed during the winter of 2017-2018, in collaboration with the Biomechanics group at the department of Biomedical Engineering in Lund.

There are some people we would like to thank for their support during the project.

First of all, we wish to thank our supervisors Lorenzo Grassi and Hanna Isaksson for all the support throughout the project. We would not have been able to do it without your help and inspiration. We would also like to thank Sami Väänänen (Department of Applied Physics, University of Eastern Finland, Kuopio) for always being available for consultation and help during the project.

We also want to give a special thanks to the people of the Biomechanics group, who we have had the fortune of working alongside during these months.

Abbreviations

BMD Bone Mineral Density.

CT Computed Tomography.

DICOM Digital Imaging and Communications in Medicine.

DXA 2D Dual-energy x-ray Absorptiometry.

GPA Generalized Procrustes Analysis.

ICP Iterative Closest Point.

OA Osteoarthritis.

OP Osteoporosis.

PCA Principal Component Analysis.

SSAM Statistical Shape and Appearance Model.

SSM Statistical Shape Model.

TPS Thin-Plate Splines.

Contents

Chapter 1

Introduction

Medical conditions associated with the hip, such as Osteoarthritis (OA) and Osteoporosis (OP), can heavily reduce life quality and expectancy [1, 2]. Pain and lack of mobility are two main concerns for those affected and both conditions are common among elderly. It is estimated that 10% of men and 18% of women aged 60 years and older have symptomatic OA [3] and that more than 200 million people worldwide suffer from OP [4]. The hip is constantly subject to loading during daily activities and the two bones which determine its functionality are the pelvis and the proximal part of the femur.

OA and OP are diagnosed based on 2D radiographic images. OA by radiological measures of the bones from plain x-rays and OP by calculation of Bone Mineral Density (BMD) from 2D Dual-energy x-ray Absorptiometry (DXA) images. The downside of the images is that they contain information in only two dimensions. The difficulty of extracting radiological measures in a 2D image will depend a lot on in which angle the image was taken, and determining BMD values in a 2D image will give an areal value with an unknown distribution. Therefore Computed Tomography (CT), which provides a 3D image, would be preferable to use. CT is a reliable visualization tool, but there is a downside of higher costs and exposure of radiation to the patient as compared to regular 2D scans [5].

This study is part of a larger project being performed by the Biomechanics group at Lund University to assess and evaluate the risk of developing OA and OP. The ongoing project includes the creation of a 3D model of the hip from a 2D image and the creation of Finite Element Models [6, 7]. The approach is to use statistical models to describe the shape

and density variation of a given population. Statistical models which can be used for this purpose are Statistical Shape Models (SSMs), which describe the shape variability within a population, Statistical Appearance Models (SAMs), which describe the density variability, and Statistical Shape and Appearance Models (SSAMs), which describe both the shape and density variability. These types of models can in turn be used to generate a 3D model of the bone from a set of 2D images by fitting the statistical model to patient-specific data [8], thus bypassing the need for CT.

At present there exists a SSAM for the proximal part of femur but not for the pelvis. A model of the pelvis is needed to be able to implement a full 2D to 3D reconstruction of the hip.

1.1 Objective & Aim

The aim of this thesis is to develop a SSM for the human pelvis and evaluate its quality and accuracy in terms of the ability to represent the shape of a male or female bone and to reconstruct a shape within or outside of the training set. The SSM can be further developed into a SSAM.

1.2 Authors' contribution

The work in this thesis was divided into two main parts, one focusing on image analysis and one focusing on programming. Therese Johansson has been responsible for the programming and Jenny Tiliander has been responsible for the image analysis. The responsibility areas have helped make the process more efficient, but collaboration and support has also been important during the project. Writing the report has been divided equally between the two authors.

Chapter 2

Background

In this section, the theory behind the project is presented. Initially, the anatomy and function of bone with focus on the hip area will be described and medical conditions connected to this region outlined. Various mathematical methods used during the preliminary work and in the creation of the SSM will be presented and definitions in mesh modeling of bone will be given.

2.1 Bone & Joints

Bone is a dynamic tissue in the human body that provides mechanical support, protects vital structures, facilitates the production of new blood cells and helps maintain mineral stability within the body. On a microscopic level it contains a collagen matrix with hydroxyapatite crystals in addition to bone cells which help remodel bone continuously. On a larger scale, bone is made up of cortical and trabecular bone. The cortical bone is compact and dense and forms the outer shell of the bone, whereas the trabecular bone is porous and generally surrounded by cortical bone. In a healthy human bone, the organization and distribution of these two bone types maximizes the absorption of energy and minimizes the trauma to the bone structure itself [9]. This is an important property as bone is regularly exposed to loading.

The location where one bone meets another bone is called a joint. Two bones are connected by ligaments. Ligaments are elastic bands of connective tissue that are strong in tension and thereby support and limit the joint's movement. Cartilage is located on the bone surfaces inside the joint and helps reduce friction between the bones during move-

ment. A synovial membrane envelops the joint and secretes a lubricating fluid into it [10].

One of the most important joints in the human body is the hip joint, which connects the upper body to the legs (see figure 2.1). It is a ball-and-socket synovial joint which connects the femur and pelvis bones [11].

Pelvis

The pelvis (see figure 2.2) is comprised of the left and right hemipelvises joined together by the sacrum and the pubic symphysis. Each hip bone is split into three partitions: ilium, ischium and pubis. The ilium is the top part of the bone, possessing the largest area of the three. Located below, the ischium holds the most strength and makes up the bottom part of the bone. The pubis joins the bone to the pubic symphysis. Initially, these three are separate bones that develop into one during growth from child to adult. Together they form the acetabulum - the hip joint connecting the pelvic bone to the femur [13].

2.2 Medical conditions affecting the hip

The hip can be affected by various diseases. Two such conditions, Osteoarthritis and Osteoporosis, will be further described in this section.

Osteoarthritis

The most common form of joint disease, Osteoarthritis (OA), leads to breakdown of the cartilage. It is an age-related disease. Thus it is more common in elderly and approximately 85% of individuals aged 75 years or more have radiographic or clinical evidence of OA [14]. As the cartilage gradually breaks down it can lead to pain, swelling and difficulty moving since the underlying bones start grinding against each other. OA is diagnosed by a combination of radiographic evidence and incident pain. Using radiographic evidence alone may lead to false negatives as OA does not always show on radiographs [2]. Hip pain can also be difficult for the patient to classify as it can appear in another location, such as the thigh or knee, in conjunction with a sharp or dull ache [15]. Therefore, novel approaches to diagnosis of the disease are needed, as well as methods to predict who may have a higher risk of developing OA later in life.

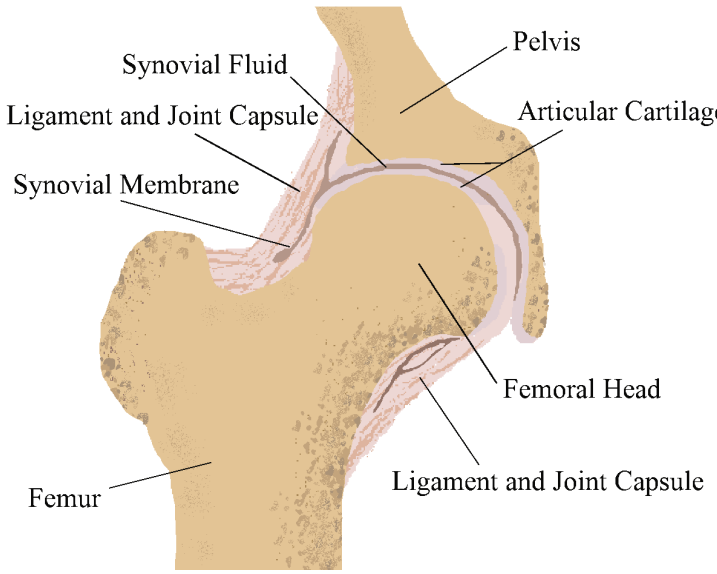

Figure 2.1: The anatomy of the hip joint. Redrawn with inspiration from [10].

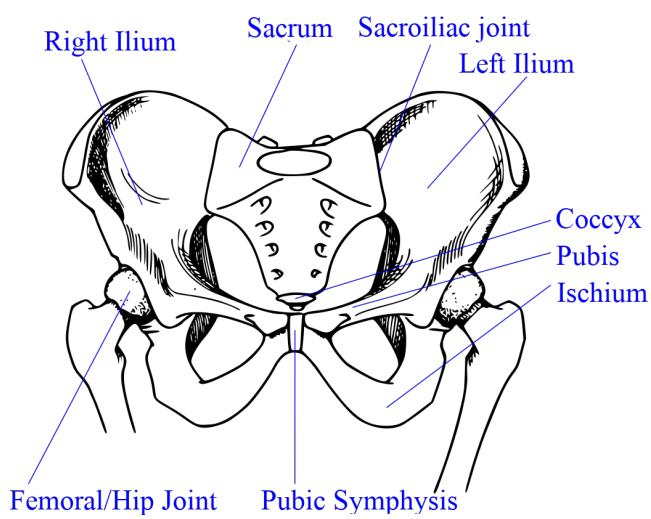

Figure 2.2: The pelvis [12].

Treatment for hip OA includes lifestyle change, pain medication and surgery. Lifestyle changes could be weight loss, walking with a cane to reduce weight on the hip, or moderate exercise. Depending on the quality of the hip, a joint replacement surgery may be recommended.

Osteoporosis

Osteoporosis (OP) is a disease which leads to reduced bone mass and an increased risk of bone fracture. The most common reason for elderly to get admitted to an acute orthopedic ward is a fractured hip [16]. These fractures generally take place in the proximal part of the femur. It is quite uncommon for the pelvic bone to fracture, but it can happen for both moderate and severe trauma [17]. Diagnosis of OP is achieved by measuring bone density. These measurements are acquired using DXA and the bone is classified as osteoporotic when the BMD is more than 2.5 standard deviations below the mean BMD of young adult women.

Treatment for OP includes lifestyle changes and medication. There are no symptoms before a fracture occurs, therefore early diagnosis is important. Patients at high risk are imaged with DXA, although apart from the BMD, the geometry, bone structure and orientation of the pelvis and the femur also has an impact on whether a fracture will occur [6].

2.3 Imaging of the hip

In this section the imaging methods DXA and CT will be presented shortly, as well as the Digital Imaging and Communications in Medicine (DICOM) saving format.

The technique behind DXA is to take two 2D x-ray images using two different energy levels of the x-rays, one with high energy and one with low energy. The image can then be used to calculate the BMD, provided that it is properly calibrated with a phantom [5].

CT is used to generate a 3D image of the hip for example when planning hip surgery. The CT image is produced using x-ray projections of the patient from a large number of views. Compared to 2D x-ray imaging, CT is more expensive and exposes the patient to more radiation. At the same time, CT includes more data as it provides information in a third dimension [5].

The image format used for storing CT images is DICOM, which is a standardized format often used for storage of medical images [18]. A DICOM contains not only the image itself, but also other information, such as patient age or radiation dose, stored in tags with a specific tag number for specific information.

2.4 Mathematical Models

The following sections will present the mathematical methods used during the preliminary work and the creation of the SSM.

2.4.1 Iterative Closest Point

The Iterative Closest Point (ICP) algorithm is a matching algorithm used to align two point clouds. For each data point in one set, the nearest point in another set is found and the distance between them is calculated. A transformation which minimizes the distance is performed and this process is repeated iteratively until convergence of the distance error is reached or for a set number of iterations. ICP was originally introduced in 1991 by Chen and Medioni [19] and independently by Besl and McKay [20]. It has since then been refined by researchers and there are numerous different versions [21]. There are several methods to speed up the selection of nearest points such as k-d trees and sampling of points [22]. There are also various methods to avoid local minima, for instance by weighing or removal of outliers. The ICP can solve:

- **Rigid Transformation** - The combination of translation and rotation. Translation is the shifting of each point by the same distance in a given direction and rotation is a translation around a fixed point.

- **Similarity Transformation** - Rigid transformations with isotropic scaling. This represents the expanding or diminishing of the point set size by a scaling factor.

- **Affine Transformation** - Rigid transformation with anisotropic scaling (a different scaling factor for each axis) and shear. Shear is the displacement of each point based on its distance from a line parallel to the direction of the displacement.

2.4.2 Thin Plate Splines

Thin-Plate Splines (TPS) is a spline (a curve which connects data points) function used in surface interpolation over scattered data. With knowledge of the movement of a set of points from one location to another, this method finds a description of the deformation of the entire object. The method is well used within medical imaging as a registration method.

For a linear and a non-linear part, coefficients are calculated which are then used to determine the TPS mapping. The resulting deformation corresponds to the deformation of a thin sheet of metal. It is achieved by minimization of the energy needed to bend the sheet of metal on the point constraints, hence its name [23].

2.4.3 Generalized Procrustes Analysis

The theory behind Generalized Procrustes Analysis (GPA) was first published in 1975 by J. C. Gower and is a method used for removing similarity transformations between shapes of objects, such as translation, rotation, scaling and reflection [24]. Let L_i be a set of data points for the shape of object number i and let $R_j^{(i)}$ be the j:th point of L_i. The task of GPA is to minimize the sum of the distance between corresponding data points in the whole set of shapes, which is done by minimizing

$$e = \sum_{j=1}^{M} \sum_{u<v}^{N} \|R_j^{(u)} - R_j^{(v)}\|^2. \tag{2.1}$$

N is the number of shapes and M is the number of points [6]. The $\|\cdot\|$ is the Euclidean vector norm which in the 3D case is calculated according to

$$\sqrt{x^2 + y^2 + z^2}. \tag{2.2}$$

2.4.4 Principal Component Analysis

Principal Component Analysis (PCA) is a method used to reduce dimensionality of large data sets, while minimizing data loss, by creating new uncorrelated variables which maximize variance [25]. It was presented in 1901 by Karl Pearson [26]. Nearly 30 years later it was independently described by Harold Hotelling [27]. In PCA all of the data is

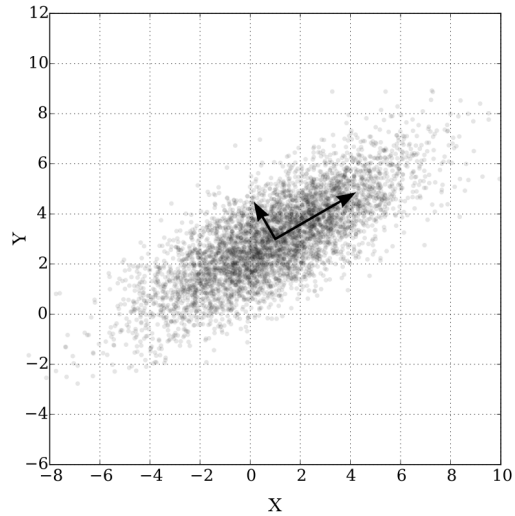

Figure 2.3: Gaussian scatter where the directions represent the principal components associated with the sample [28].

collected in a matrix X where each column has data from one subject and each row has all the data concerning one variable. To successfully perform PCA, the mean is subtracted in order to center the data.

A transformation to an orthogonal coordinate system is found, such that the new coordinate system will have axes in the direction of the maximum variance. The first axis will point in the direction of maximum variance, the second axis orthogonal to the first one in the direction of the second largest variance and so on (see figure 2.3). The solution to the PCA is given by solving the eigenvalue problem of the covariance matrix of X. As such, the principal components are calculated and sorted by the largest eigenvalue, corresponding to the highest variance, is the first principal component. By lowering the amount of principal components used, the dimensionality of a large data set can be reduced.

2.4.5 Statistical Shape Models

A Statistical Shape Model (SSM) is a model of a certain object made in 2D or 3D, representing its shape by a mean shape and different kinds of variation in so called modes [14]. There are several steps in the creation of this kind of model and they are briefly presented here.

Landmarks

A major factor which influences the model quality is the correspondence of the shapes in the training set [8]. Thus, it is necessary that all objects included in the model are identically defined. This can be restricted in the SSM by the use of landmarks. An anatomical landmark is a location which corresponds to the same anatomical location on each shape. These can be chosen by having a trained person set the landmarks on each training shape, though when working in 3D with a large number of training objects this procedure will consume a lot of time and introduce variability. Thus, automatic ways of setting landmarks are preferable, especially when working with a lot of data. If the shape is simple, it could be enough with a few landmarks but if the shape is more complicated, more landmarks will be needed to represent it.

Creation of a SSM

After the chosen landmarks on all available training data has been defined and correspondence between the subjects has been established, the variation depending on rotation, translation, scaling and reflection is eliminated from all objects [6]. As similarity transformations do not affect the shape itself, they should not be included in the model [8]. The most widely used algorithm for achieving this is the GPA (section 2.4.3). A mean shape is computed according to

$$\bar{\mathbf{x}} = \frac{1}{N} \sum_{i=1}^{N} \mathbf{x}_i, \tag{2.3}$$

where N is the number of training objects, $\mathbf{x}_i$ is the training object for patient i and $\bar{\mathbf{x}}$ is the mean shape of the training objects.

By performing PCA (section 2.4.4) on the landmarks one can determine which variances are of significant importance. These variances are called modes, ϕ_i. The outcome of the SSM is the mean shape $\bar{\mathbf{x}}$ and the modes ϕ_i. These can be used to describe shapes present or not present in the training set by

$$\mathbf{x} = \bar{\mathbf{x}} + \sum_{i=1}^{c} b_i \phi_i. \tag{2.4}$$

The b_i values describe the contribution of the mode ϕ_i in the c number of chosen modes.

Leave-one-out

The leave-one-out method can be used to evaluate the ability of the SSM to represent shapes that are not in the current training set [29]. Out of the available shapes, all except one is selected to be the training data for the SSM. The shape not included in the SSM is then reconstructed using the c number of chosen modes. The most suitable b is calculated by

$$\mathbf{b} = \phi(\mathbf{x} - \bar{\mathbf{x}}), \tag{2.5}$$

where $\mathbf{x}$ is the left out shape. ϕ and $\bar{\mathbf{x}}$ are the modes and the mean shape from the SSM created with $N - 1$ shapes. The best approximation of the unknown shape x is then calculated by

$$\mathbf{x} \approx \bar{\mathbf{x}} + \mathbf{b}\phi. \tag{2.6}$$

How similar this is to the real shape can be used as a measure of how good the SSM is at describing a shape not present in the training set.

Usage of SSM

One of the most common uses for a SSM is image segmentation. It is widely used in research for image segmentation of especially brain and cardiac structures. One of the advantages of using a SSM when segmenting is that the biological variance is included in the model. This of course requires that the training data for the SSM is large enough to represent the population. SSMs are also used for shape analysis when correlating shape to medical conditions. For femur and pelvis there are several studies where it has also been used to extrapolate geometry from sparse 3D data for surgery [8].

2.5 Mesh Representation

A mesh is a digital way of representing an object in 3D. There are two different kinds of meshes that will be used in this project and which will be explained in this section - triangular surface meshes and tetrahedral volume meshes [30].

Surface Mesh

A triangular surface mesh is used to represent the surface of a shape, e.g. the outer surface of the pelvic bone. A surface mesh consists of nodes and elements. Nodes are coordinates located at the surface of the shape, often with a predefined approximate distance between them. The distance between the nodes should be chosen small enough so that the mesh is able to resolve the topology of the shape, but not too small since it will require too much computer power to handle. A smaller distance between the nodes results in a finer mesh and a larger distance between them results in a coarser mesh. The surface of an object is defined by triangular elements. A triangular element is defined by 3 nodes. In figure 2.4, an example of a surface mesh can be seen to the left.

Volume Mesh

A volume mesh also consists of nodes and elements. These nodes are the same as nodes on a surface, except a volume mesh also contains the internal structure of the object. This is done by the addition of nodes in the internal part of the object and the use of tetrahedral elements instead of triangular elements. A tetrahedral element is defined by 4 nodes. Just like for the surface mesh, the fineness of the mesh is decided by the distance between the volume nodes. In figure 2.4, an example of a volume mesh can be seen to the right.

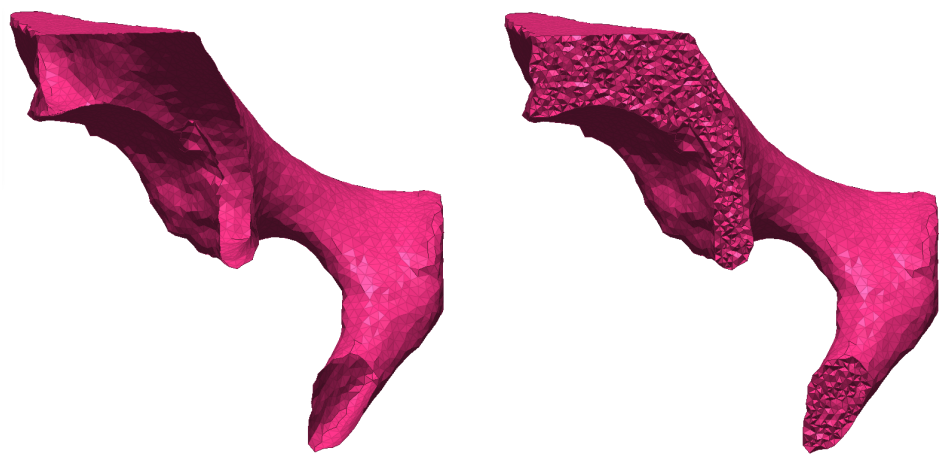

Figure 2.4: Example of a surface mesh (left) and a volume mesh (right).

Chapter 3

Material & Methods

In this chapter, the material will be presented and the methodology outlined. In summary, the sections below contain the following:

- **Material** - Information about the DICOM images, already available segmentations, and code provided from previous studies.
- **Segmentation** - How the segmentation of the DICOM images was made.
- **Template mesh** - How the template surface mesh and the template volume mesh was created.
- **Registration of target bones** - How the patient anatomy was represented using the template surface mesh and the template volume mesh.
- **Creation of SSM** - How the SSM was created from the registered bones, and how the SSM was evaluated.

3.1 Material

The images used in this study are CT images of patients with OA scheduled for hip joint replacement prior to operation, taken with a CT device and parameters according to table 3.1. The bones included in this study are intended to be contralateral to the hip that needed to be replaced. This indicates that the bones used are defined as not in need of hip joint replacement, although it cannot be ensured that all bones are perfectly healthy. For the majority of the bones, information about the side to

Table 3.1: CT device and its parameters [6].

Device	Philips Ingenuity CT
Tube Voltage (kV)	140
Exposure (mAs)	63
$CTDI_{vol}$ (mGy)	6
Resolution (mm)	0.5-0.9

use was already defined from a previous study [31]. The ethical permission was granted by The Ethics Committee at Lund University, Faculty of Medicine, permission 2009/369.

In table 3.2, information of the patients used in this study is presented. For most patients, segmentations of the pelvis were available from a previous study [31].

Table 3.2: Patient images used in this study.

Gender	**Age, mean±SD (min-max)**	**n**
ALL	58±8 (39-74)	47
M	60±8 (46-74)	26
F	55±7 (39-65)	21

Aside from the segmentations, the larger project that this study is a part of has provided MATLAB (MATLAB R2017b [32]) code to use in creation of the SSM for pelvis. The MATLAB code is object-oriented and was used to create the statistical model of femur. During this study, the code has been used as a basis for the creation of a SSM for pelvis.

3.2 Methods

In this section, the methodology will be presented. An overview is illustrated in figure 3.1. The method follows the same structure as the one that was used to create the femur model, but has been adapted to the pelvis.

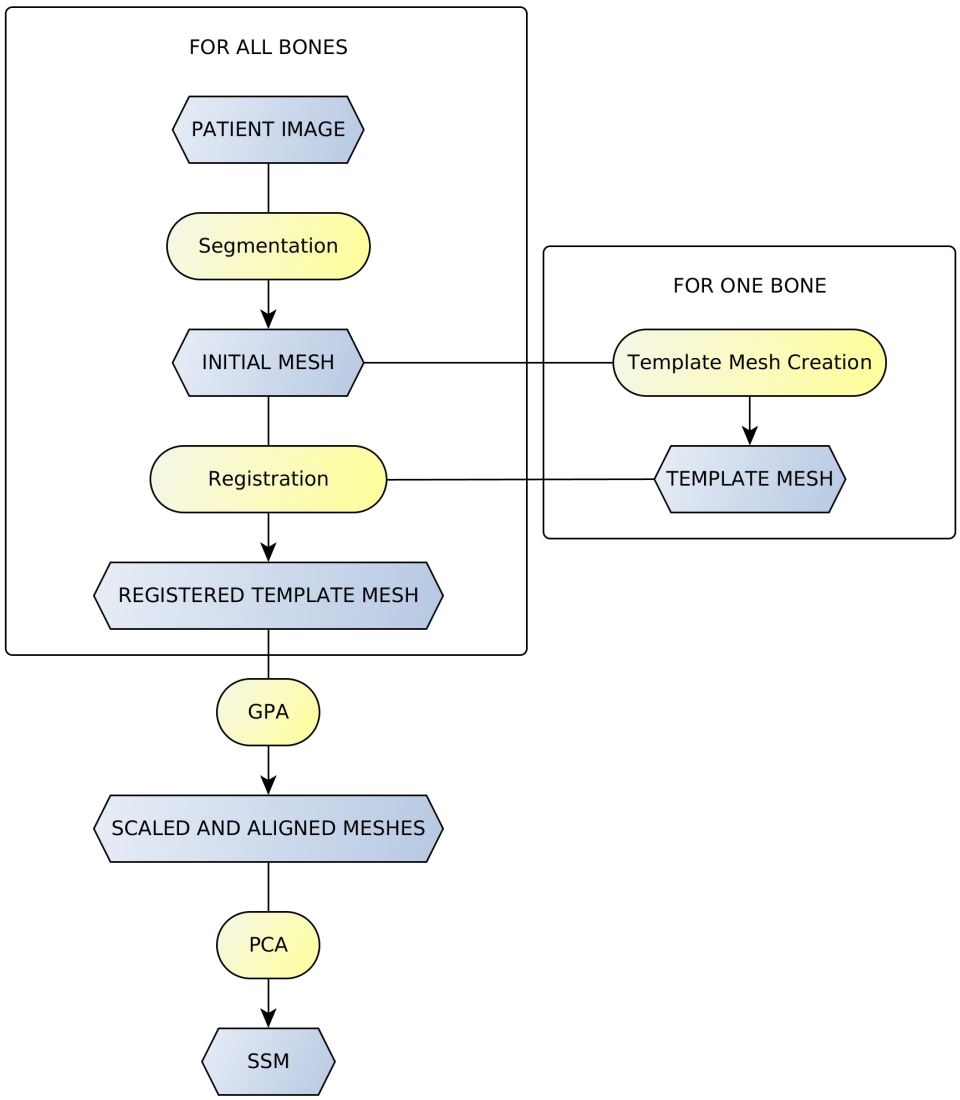

Figure 3.1: Flowchart over the steps of the study.

3.2.1 Segmentation

As the purpose of this study was to create a SSM that could describe the pelvic shape more accurately than in the previous study, the available segmentations were examined to determine which segmentations needed improvement. The quality and accuracy of the available segmentations were investigated in Seg3D (Seg3D 2.4.0 [33]) by displaying the segmentation masks on top of the DICOM images and viewing one slice at a time, see figure 3.2a. For the bones which did not have the side to use previously defined, the DICOM images were viewed close to the hip joint to determine which side to include in the model.

The extent of the improvement of the segmentations depended on the nature of the error. In some cases it was enough to manually adjust a few slices and in other cases the whole segmentation was recreated from the DICOM images.

For small adjustments in a few slices, the paint brush tool in Seg3D was used. Remaking of a segmentation from the beginning was done using several filters and tools in Seg3D. A gaussian filter was used to remove noise and thresholding was used to select the region of interest (pelvis). Morphological operators such as dilate and erode, connected components and fill holes were also utilized to make the segmentation. Image 3.2b shows a 3D view of the initial segmentation in blue and the improved segmentation in yellow.

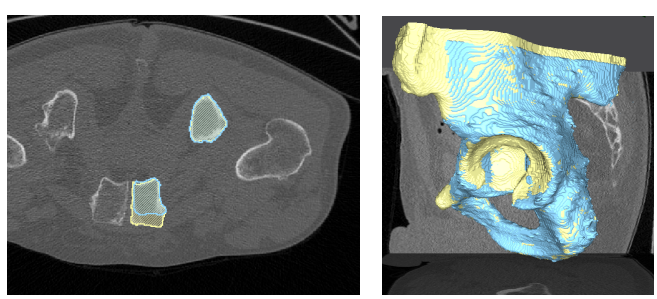

(a) Axial view (b) Volume view

Figure 3.2: An example of a segmentations where changes were made. The changes are in yellow and old segmentations in blue.

Before exporting the segmentation, it was cut in a transverse plane which was aimed to be in the same anatomical place for all the target bones, see figure 3.3. This was done to make sure each bone included the same anatomy as all patient scans had varying cut-off locations.

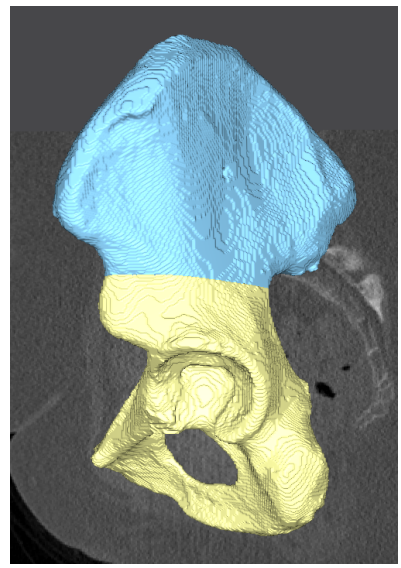

Figure 3.3: The location where all segmentations were cut off (where the segmentation goes from yellow to blue).

3.2.2 Template mesh

The nodes used as landmarks in the SSM were defined in a template mesh. From the available patient bones a male left pelvis was randomly selected to serve as template.

The segmentation of the selected patient was smoothed in the software Stradwin to remove irregularities (Stradwin 5.3 [34]). The smoothed pelvis was thereafter meshed into a triangular surface mesh using the iso2mesh plugin in MATLAB. An endocortical (or inner) surface, surrounding the trabecular bone but not the cortical bone, was found with the thickness mapping tool CBM v2 in Stradwin [35]. This endocortical surface, containing the same number of nodes as the outer surface, had to be modified to be of any use in the volume meshing, since it intersected itself several times. A MATLAB script was therefore created to remove problematic intersecting parts, see figure 3.4. A tetrahedral volume mesh was then created from the surface mesh (HyperMesh 2017.2 [36]). The endocortical surface was used when creating the volume mesh to be able to later track which elements belonged to the trabecular and which elements belonged to the cortical bone.

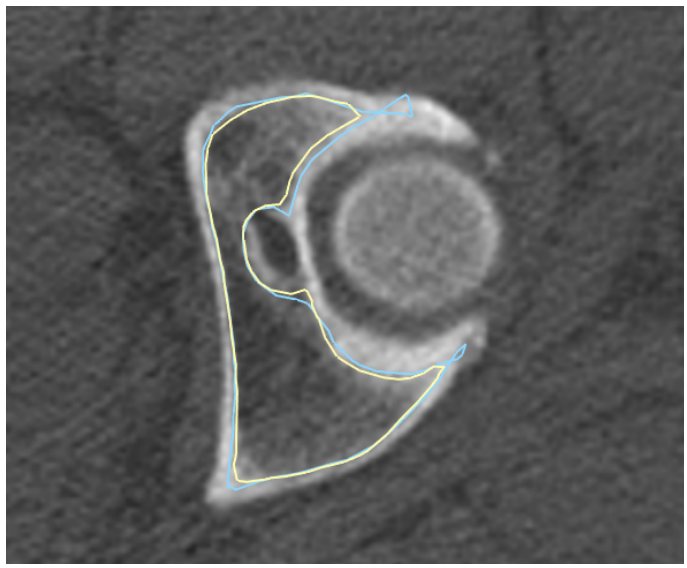

Figure 3.4: An example from Stradwin where the endocortical surface intersects itself (blue). The yellow line is the modified inner surface without intersections.

3.2.3 Registration of target bones

To ensure that the nodes of the target objects to be included in the SSM were defined equally, the template mesh was registered to each target bone. The initial registration was performed on the surface nodes of the mesh. This result was thereafter applied in TPS of the volume nodes. During the deformation of the template mesh, the top area surface of the bone, where it had been cut, was not included - any nodes located in this area were removed during registration of the target bone.

Registration of the template surface mesh

If the target bone was from the contralateral body side as compared to the template mesh, the template was first mirrored. 1000 of the surface nodes were then used in affine registration to align the template and the target mesh. The surface nodes were chosen randomly from the nodes in the initial surface mesh derived from the segmentation of the target bone.

Subsequently, the target nodes were moved closer to the template mesh by alignment of the middle points of the two bones. The middle points were calculated by taking the height of each bone in z-direction

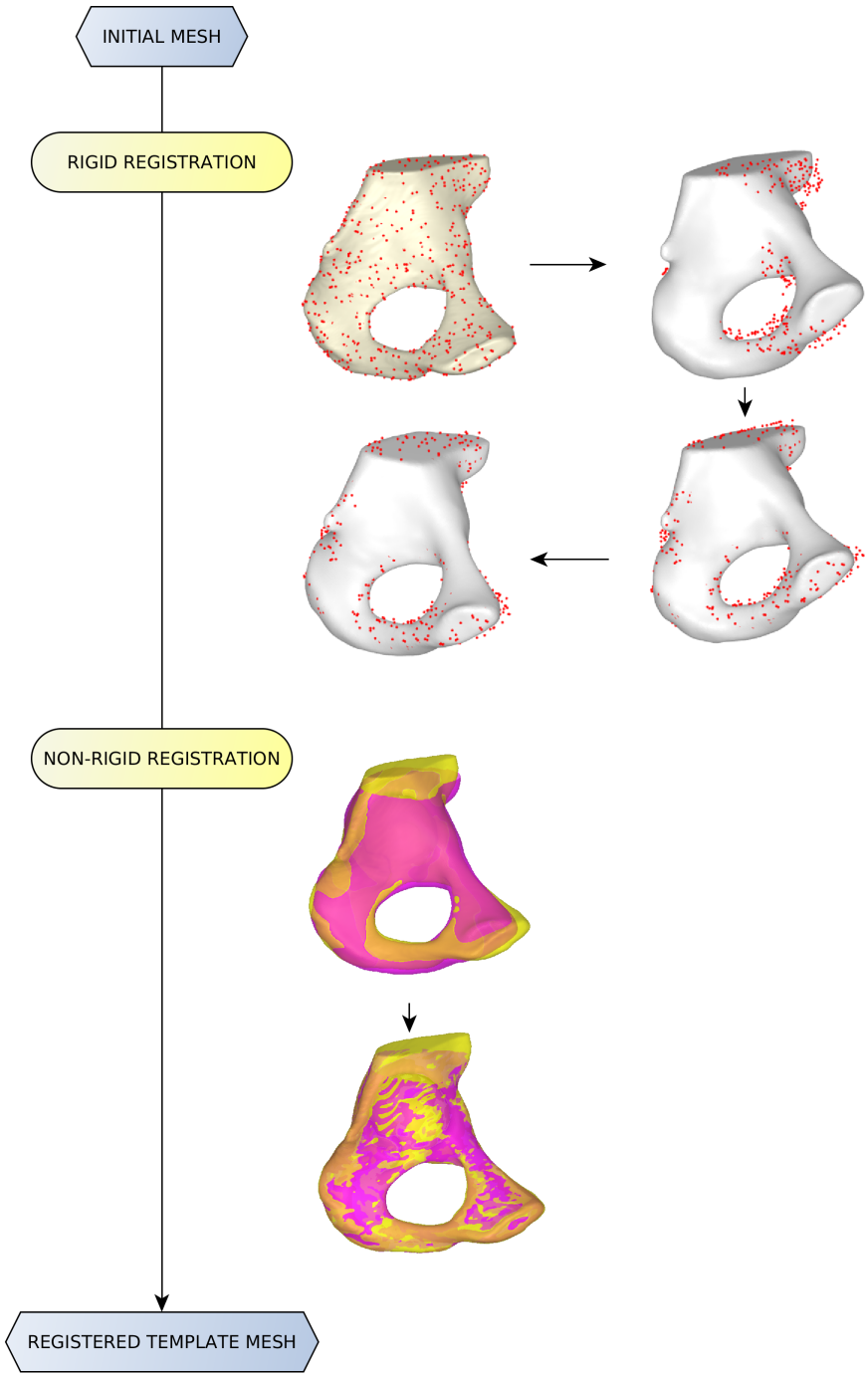

Figure 3.5: Registration of the template surface mesh. The yellow mesh is the initial segmentation, the white mesh is the template mesh and the mesh in magenta is the registered template surface mesh.

and finding the mean coordinate. Affine registration of the bones was performed utilizing an ICP (section 2.4.1) function with finite difference methods [37]. The registration was made step wise to be able to monitor the changes and confirm that it was done accurately. First, translation and rotation was used, followed by rigid- and resize transformation. The resulting point cloud was registered with an optimizer, which searches for the minimum of the function, using the previous four registrations with the addition of shear. A filter was created for the end result of all previous transformations. Finally, an inverse of this filter was used on the template mesh to get the registered mesh, see the upper part of figure 3.5.

A problem occurred in the registration of the lower arc shape of the pelvis (ischium) for some of the bones. For these bones it could not be correctly identified which side of the ischium to register the nodes to. This was corrected by performing an additional alignment of this region for the bones affected. The alignment was accomplished by defining the arc region of the mesh and then performing ICP on that area separately from the rest of the mesh.

After the affine registration, a non rigid ICP function [38], using seven iterations, was used to deform the template mesh to the target mesh. TPS (section 2.4.2) was then used on the deformed template utilizing 1500 random surface points, see the lower part of figure 3.5. Afterwards the mesh was smoothed, the intersecting elements repaired and the surface normals computed. To validate the results, the mesh was imported into Stradwin and compared to the original DICOM images by visual inspection. The comparison was done to determine that the registration process had been successful and that the mesh was ready to be used in the next step of the process.

Registration of the template volume mesh

A subset of 2000 random nodes of the registered mesh were used for the volume transformation. According to the deformation of these nodes, TPS was performed on the volume nodes. The results were evaluated by comparison of point-to-surface distance to the original segmentation.

3.2.4 Creation of the SSM

The SSM was created using all available data for both male and female patients. Translation and rotation between the bones was first elimi-

nated from the training set through GPA (section 2.4.3). GPA was also used to normalize the scaling for all training bones. The normalization is an important step to guarantee that the difference in size within the training set will not affect the results. The nodes of all subjects were then collected in one matrix, the mean was removed from the data and PCA was run.

A SSM for all female patients and one for all male patients were also created to be able to investigate the differences in mean shape between the genders.

3.2.5 Evaluation of the SSM

The model was evaluated by analysis of the modes of variation and the resulting mean shape of the SSM. The statistical difference in mode variation was investigated between the various modes but also to explore disparity between the male and female shape of pelvis. The Kolmogorov-Smirnov test was used to assess normality of the distributions, and a two-sample t-test was used to evaluate if the male and female distributions were independent from one another. Both tests were performed at a 5% significance level.

Reconstruction of bones within the training set was performed using both the full set of modes and a reduced set. For the reduced set, the resulting variances from the PCA were added up to a tolerance of 95%. The reconstruction with a reduced amount of modes was evaluated by comparison of the point-to-surface distance to the reconstruction using the full set of modes.

The SSM was also evaluated using the leave-one-out method described in section 2.4.5. The bone which was left out was compared to the reconstruction of itself. This was done by calculating the point-to-surface distance from the surface nodes of the reconstructed bone to the surface of the original bone. Leave-one-out was done for all of the bones in the training set and point to surface distances were calculated for each of them.

Chapter 4

Results

The figures presented in this chapter are based on the average score of all bones used in the SSM. The average errors were calculated by performing Root Mean Square Error in each node for all meshes. The mean and the standard deviation were calculated from the values of all nodes in all bones.

4.1 Template mesh

The surface mesh element size was set to 1 mm, which resulted in a surface mesh with 25970 nodes and 51940 triangular elements. The element size of the volume mesh was set to 2 mm and resulted in a mesh with 62531 volume nodes and 347947 tetrahedral elements. The template volume mesh is shown in figure 4.1. The template contains information of which nodes are located on the top surface, where the cut-

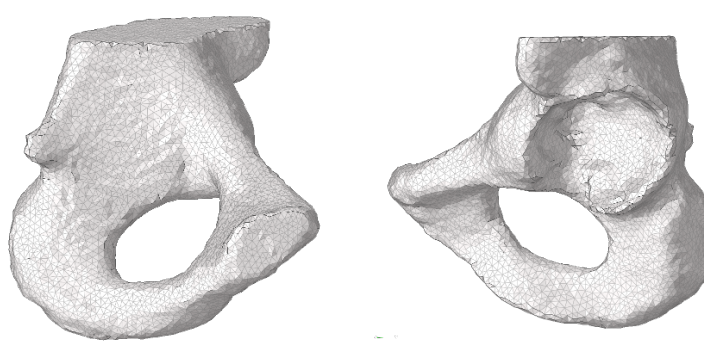

Figure 4.1: The template volume mesh from two different views.

off point was set, for both the surface mesh and the volume mesh. The template also contains information of which elements from the volume mesh belong to the cortical part of the bone and which belong to the trabecular part of the bone. Information about which volume nodes that are located on the surface is also available.

4.2 Registration of target bones

The registration of the template volume mesh was evaluated by calculation of the distance from each surface node of the registered mesh to the surface of the segmented shape. The distance is illustrated in figure 4.2. The mean error was 0.42 ± 0.27 mm (1-2 pixels) the maximum being 5.29 mm. The largest error was located just below the ischial spine of the ilium.

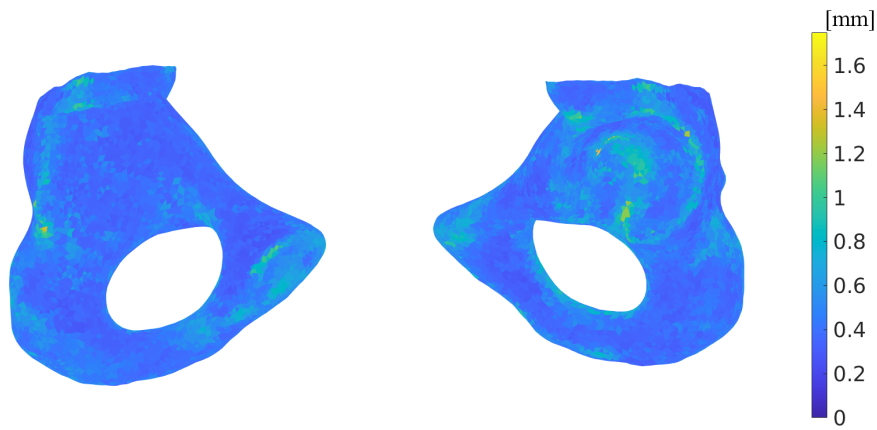

Figure 4.2: The average point to surface distance error between the registered volume mesh and the initial segmentation.

4.3 Statistical Shape Model

Modes

The first four modes (accounting for 68 % of the model variation) are visualized in figure 4.4. All modes were tested with Kolmogorov-Smirnov to check for normal distribution of male and female distributions. The hypothesis of normal distribution could not be rejected in any of modes at a 5% significance level and the modes were therefore considered to be normally distributed. All modes were also tested for significant difference between the male and female distribution which was found in mode 1 and 3. The mode variation for mode 1 and 3, representing 32 % and 11 % of the variation respectively, is illustrated in figure 4.3.

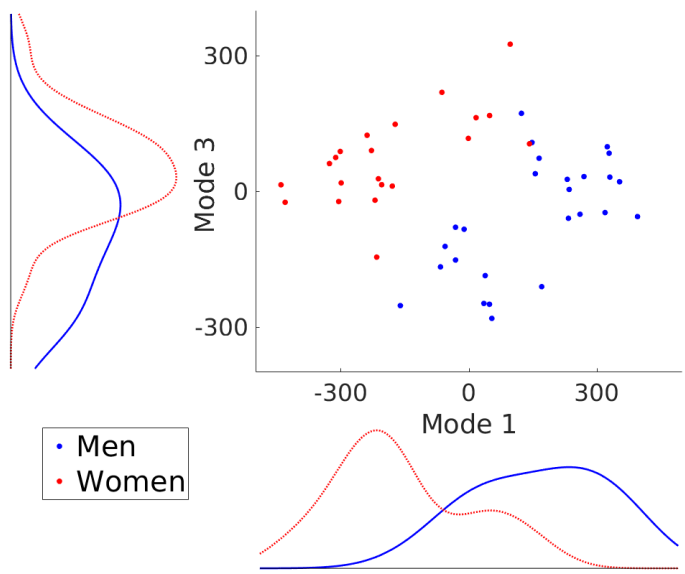

Figure 4.3: The mode variation of mode 1 and mode 3.

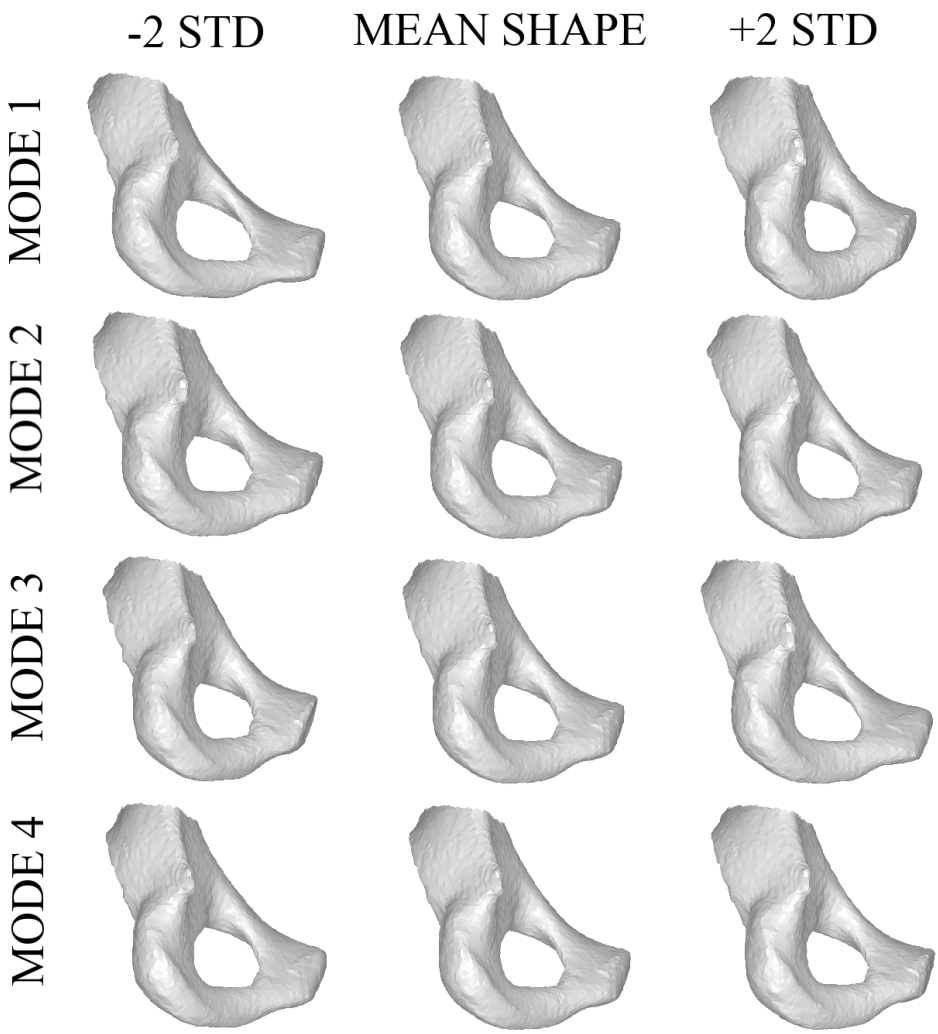

Figure 4.4: The shape variation of mode 1-4 of the SSM.

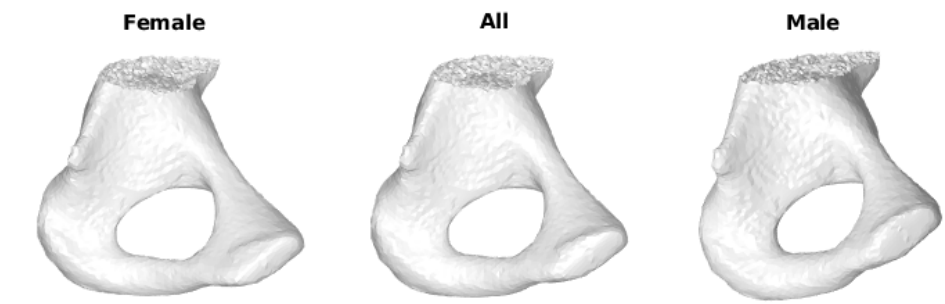

Figure 4.5: The mean shapes of the female, full and male SSM.

The morphological differences between the subgroups were also evaluated by the creation of SSMs for the male and female bones separately. The mean shapes of these SSMs were visualized and are presented in figure 4.5.

Reconstruction

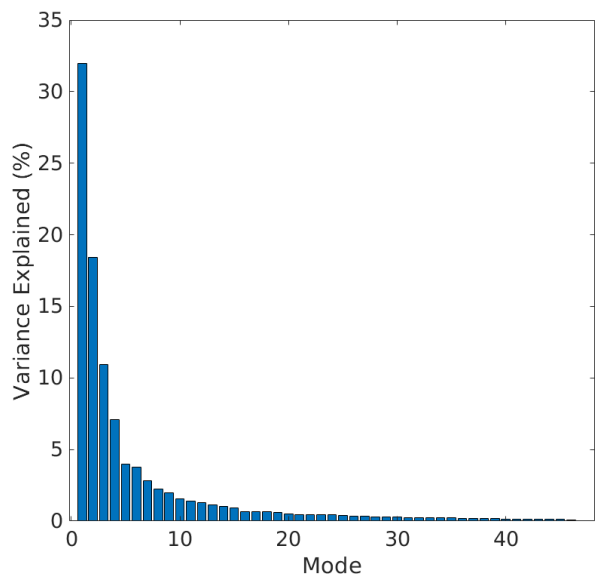

Figure 4.6: The variance representation of each mode of the SSM.

24 modes were needed to account for 95 % of the variation, see figure 4.6. The result of a reduced reconstruction using 24 modes in

comparison to the full reconstruction is presented in figure 4.7, which shows the distance error from each node in the reduced reconstruction to the surface of the full reconstruction. The mean distance was 0.80 ± 0.59 mm. The maximum distance was 5.41 mm.

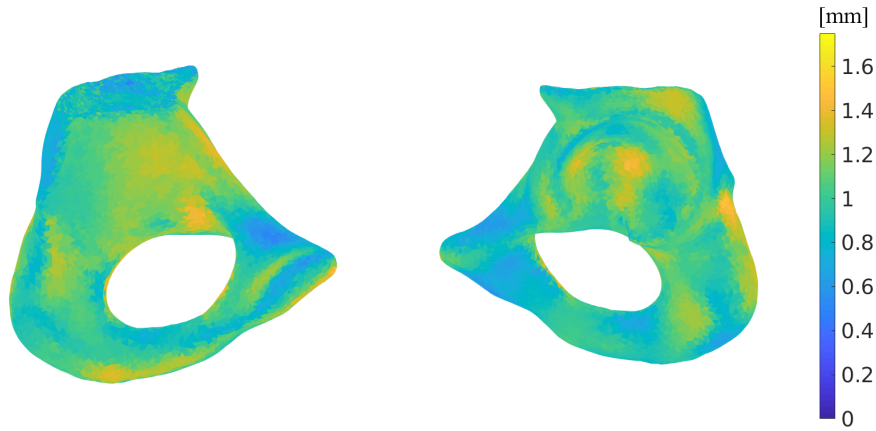

Figure 4.7: The point to surface distance error between the reduced and full reconstruction.

Leave-one-out

For the 47 SSMs that were created during the leave-one-out method, the number of modes needed to account for 95 % of the variation was 23 in 43 cases and 24 in 4 cases. The distance difference from the nodes of the reconstructed bone to the surface of its registered template mesh is shown in figure 4.8. The surface where the cut-off plane was placed was not included in the calculation, which is why its distance error is set to zero. The mean distance was 1.17 ± 1.00 mm. The maximum distance was 9.52 mm. In table 4.1 the mean distance, standard deviation and maximum distance is presented for all the patients.

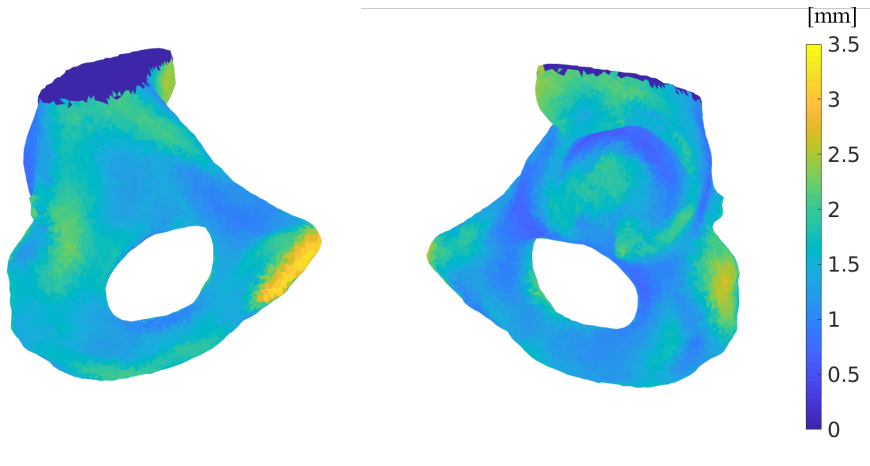

Figure 4.8: The point-to-surface distance error between the leave-one-out reconstruction and its registered template mesh. Note the color scale is different compared to previous figures.

Table 4.1: Gender, mean distance, standard deviation and maximum distance for the 47 patients.

Patient	**Gender**	**Mean [mm]**	**Std [mm]**	**Max [mm]**
1	M	0.97	0.89	5.53
2	M	1.79	1.30	6.83
3	M	1.82	1.39	8.35
4	M	1.18	0.87	4.81
5	M	1.07	0.96	5.93
6	M	1.07	0.84	5.22
7	M	1.53	1.14	5.99
8	M	0.91	0.72	4.69
9	M	1.52	1.10	5.96
10	F	0.69	0.60	4.02
11	M	1.16	1.02	7.55
12	M	1.20	1.29	9.52
13	F	1.11	0.87	5.55
14	F	1.02	0.83	5.24
15	M	1.37	1.03	5.30
16	F	0.74	0.61	4.71
17	F	0.86	0.66	4.30
18	M	1.33	0.96	5.62
19	F	1.09	0.86	5.77
20	M	1.35	1.06	6.15
21	F	0.95	0.66	4.66
22	F	1.15	0.88	5.62
23	F	1.12	0.89	6.55
24	F	1.45	1.12	6.38
25	M	1.66	1.17	5.81
26	F	0.76	0.62	3.96
27	F	1.48	1.11	7.61
28	M	0.77	0.72	4.66
29	F	0.96	0.78	6.04
30	M	1.82	1.28	7.63
31	F	0.85	0.65	4.12
32	M	0.76	0.63	4.82
33	M	1.58	1.09	5.02
34	F	0.78	0.57	3.07
35	M	0.95	0.89	5.47
36	M	1.33	1.01	5.07
37	M	1.13	0.92	5.76
38	M	1.51	1.24	6.61
39	M	1.97	1.30	6.11
40	F	0.93	0.95	7.84
41	M	0.99	0.80	5.56
42	F	0.86	0.69	5.18
43	F	0.87	0.71	4.18
44	M	1.38	1.07	6.55
45	F	1.26	1.10	6.84
46	F	0.86	0.65	3.88
47	F	0.85	0.67	3.78

Chapter 5

Discussion

The aim of this thesis was to develop a SSM for the human pelvis. A considerable amount of effort went into the preliminary work, which was divided into three main tasks, namely: segmentation, creation of a template mesh and registration of the template mesh to each bone. The SSM was evaluated by the use of statistical tests, reconstruction with a reduced model and reconstruction using the leave-one-out method.

5.1 Preliminary Work

The images used in this study were taken prior to hip replacement surgery. The aim was to create a model of a healthy pelvis. Some of the scans had previously been used in a SSAM utilized for the removal of shadowing during 2D to 3D reconstruction of femur, and the side to be used in the statistical model had been defined. In order to increase the data set, scans which were available but previously unused were included in this study. For these, the side to be used was decided upon during the project. Thus, although we intended to create a SSM for a healthy pelvis, the bones used for this study all had pathological occurrence in the contralateral hip. Since it is known that OA often occurs on both sides eventually, we cannot ensure that all hips were healthy.

The landmarks of the SSM were defined as nodes in a template mesh. Thus, the creation of a template mesh for the pelvis was essential for the study. The main requirement for the template mesh was its capability of an accurate registration to all bones within the data set. This was the case for most target bones, except for a few which needed additional alignment of the ischium. For these bones, it was apparent by

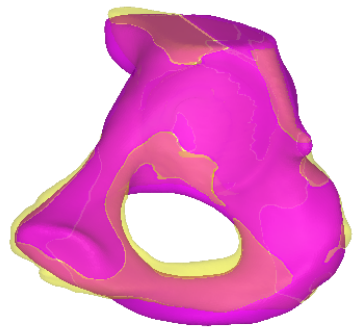

Figure 5.1: Template mesh (magenta) in comparison to the segmentation (yellow).

comparison to the CT scans and studying of the shape of the registered mesh that the lower arc of the bone had not been properly aligned. For a few bones, the resulting mesh intersected itself. During the non-rigid registration, nodes from the upper part of the ischium region of the template mesh were not correctly registered. Instead of registering to the upper part of the arc, these nodes registered to the lower part. The issue was due to the ischium of the target mesh being located superior to the ischium of the template mesh, see figure 5.1.

Necessity of additional alignment was likely due to the ischium of the template being quite thick and inferiorly located. The bone used as template in this study was from a male patient. As the thickness and length of the ischium region varies between the genders, there might not have been a problem in the registration if a female patient had been used as template, although this might have resulted in other registration issues instead. The additional registration of the region had to be done for both female and male patients, which implies that the shape can vary within the gender groups as well as between genders.

The meshes that the template was registered to were either segmentations made from scratch or modifications of the available segmentations from previous studies. One important step during this process was that each segmentation was cut off in a plane, just above the acetabulum. The purpose of the cut-off process was to assure that the anatomy included in the statistical model was roughly the same for each bone and that the registration of the template mesh was accurate.

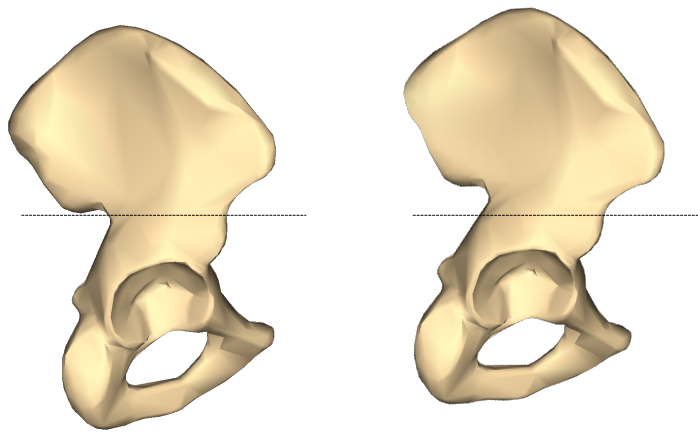

Figure 5.2: The cut-off point [39].

The cut-off point was defined mainly according to the limitations of the available scans but also considering the areas of interest of the bone. It was essential that the cut-off point was present for all patients. Ideally, the whole bone should have been included in the model, but due to the rarity of the whole pelvic bone being present in a CT scan this was not possible. The areas of interest for the SSM were deemed to be in the inferior region of the bone and especially in the acetabulum, where the pelvis connects to the femur. A possible issue that the cut-off process poses is that each bone was not necessarily cut in a straight plane due to the angle of the scan, see figure 5.2. This introduces uncertainty in this area of the mesh and also in how much of the rest of the bone is included or not included in the resulting mesh. As this top area is not technically a surface of the actual bone, and it also introduces considerable uncertainty, it was not included in the registration process.

The registration of the template mesh did not result in large distance differences to the initial segmentation. Given that the pixel size was between 0.5-0.9 mm for the CT scans, the registration in average only differed less than 1 pixel to the segmentation. The largest error was located at a region which was not of particular interest. If needed, a correction could be made utilizing an additional registration of that part of the bone, but it was not deemed necessary for the purpose of this study. For the acetabulum, inaccuracy was present across the area. It was also difficult to determine the nature of this error as the ground truth in this case was the initial segmentation of the bone. The exact boundary between acetabulum and femur was difficult to identify at the

resolution of the available images and it is therefore also possible that the segmentation of this region was not completely accurate.

5.2 Creation of the SSM

The aim of the registration process was to assure that the nodes were equally defined for all bones, so that the meshes could be used in the creation of a SSM. The first step in the creation was to align all bones to each other. During this alignment the size was normalized, meaning that the variations of the resulting modes were not dependent on the size of the bones. This was important for the study as the bones included differed considerably in size.

The complex shape of the pelvis resulted in the need of 24 modes to account for 95% of the variation within the data set. Reconstruction using a reduced model resulted in errors of around 1 pixel and the errors were also quite evenly distributed over the shape, which indicates that the reduced set of modes could be used to decrease the complexity of the problem. Further, the possibility of lowering the complexity indicates that the model could be used in applications where higher processing power is required.

The dataset used in the study was relatively small. Almost 50 % of the available modes had to be included in the reduced model to account for 95% of the variance. If more bones were to be included, it would most likely not be needed to include such a relatively large amount of modes as compared to how many modes were present.

The modes were all assumed to be normally distributed for both male and female as the null hypothesis in the Kolmogorov-Smirnov test was not rejected at a 5% significance level. In mode 1 and 3 the male and female distributions were statistically different. Visually, the variation of the modes seem to be due to the thickness and width of the bone. In comparison of the female and male mean shape, constructed in two separate SSMs, it is visible that this is the case for these shapes as well. The mean shapes generated in this study seem to be qualitatively similar to the shape of a male and female pelvis, see figure 5.3. The mean shape of the SSM including both genders suggests that the SSM was able to capture the differences of the gender groups.

The leave-one-out evaluation of the SSM shows that the model has mean errors of around 1.5 pixels when reconstructing a shape outside of the training set. This indicates that the model has potential to be

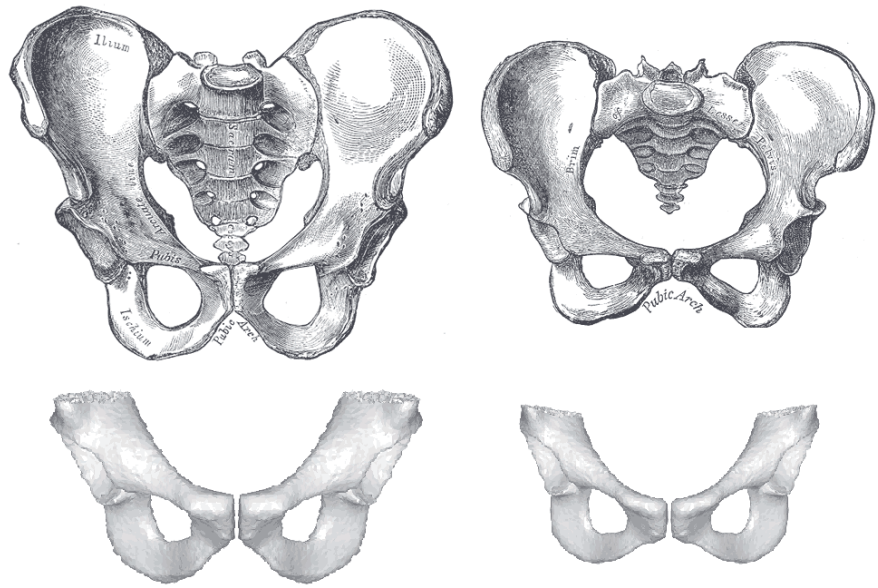

Figure 5.3: A male (left) and a female (right) pelvis [40] and the mean shapes of the two SSMs generated in this study.

improved, which could be done by increasing the amount of training bones. Comparison between the leave-one-out reconstructions of the 47 bones shows that no bone is significantly better or worse reconstructed than any other. On the other hand we can see from the average bone that the model seems to have troubles reconstructing a particular part of the pelvis, namely the pubis. The error in this area could originate from the difficulty of separating the pubis from the pubic symphysis, which arose during segmentation.

5.3 Future Perspective

The current model has, in this report, been referred to as a SSM. However, the model is prepared to be a SSAM as the template contains volume elements, and the mean shape and modes of the SSM is represented as a volume mesh. The final steps to turn the SSM into a SSAM would be to insert the correct BMD values in the meshes. Our model is prepared to do this. The addition of BMD values has not been done yet as we did not have access to the phantom calibration values used when taking the DICOM images.

To improve the model and to make it more representative, it needs more patients and the characteristics of the patients need to be scattered across the population. The patient DICOM images also need phantoms and available phantom calibration values.

The current version of the SSM is, as previously mentioned, constructed from pelvises which were cut already during the segmentation process. When working with a larger data set it would be of interest to find an automatic method to handle the cutting of the mesh and include this in the code. The angle of the cut-off plane could also be incorporated in the code to not depend upon the orientation of the pelvis in relation to the imaging angle, which could lead to a cut-off point which corresponds better in between the bones.

Another improvement would be the creation of a new template mesh from the mean shape of the current SSM. This might improve the accuracy of the registration due to a more neutral shape than the current template, which was taken from a male patient.

The template mesh used in our model contains an endocortical surface and information about which elements belongs to the cortical and the trabecular bone. This is not used in the current version of the model since the program used for segmenting the inner surface (Stradwin) had troubles creating a good endocortical surface, due to the complex shape of pelvis. If desired, the inner surface from the template could in the future be used for a more accurate prediction of the cortical density and thickness.

Our pelvis model will be used together with the SSAM for femur. These two models are created with the same structure and from code with similar characteristics. The two models together will hopefully contribute to better segmentation of the hip and to facilitate the 2D to 3D reconstruction of the hip. The 2D to 3D reconstruction could be

used to visualize the shape, density and relationship between the two bones. A vision is that the 3D visualization could be used to find new and better ways of predicting medical conditions in the hip.

5.4 Ethical Reflection

The images used to create the SSM were from patients scheduled for hip surgery, and would have been taken regardless of this study. Therefore, the creation of our model did not contribute to any additional exposure of X-rays to patients. The same images have also previously been used for several studies.

As this model is meant to contribute to a decrease of CT usage and the possibility of performing 2D to 3D reconstruction from DXA images, the exposure of X-rays to patients in the future could be reduced as a result. Another ethical advantage is the possibility of prediction and diagnosis at an earlier stage of hip disease, leading to an increased opportunity of preventive care.

Chapter 6

Conclusions

In this master's thesis a SSM for the human pelvis was developed. The generated SSM was able to accurately reconstruct the shape of pelvis independent of gender. In its current implementation, the SSM is also prepared for incorporation of BMD values. With the addition of correct BMD values the model could therefore be expanded to include appearance. Together with a statistical model of femur, the model can in the future help identify additional parameters and novel ways of diagnosis and prediction of medical conditions in the hip.

Bibliography

[1] J. Compston, A. Cooper, C. Cooper, N. Gittoes, C. Gregson, N. Harvey, S. Hope, J. A. Kanis, E. V. McCloskey, K. E. Poole, D. M. Reid, P. Selby, F. Thompson, A. Thurston, and N. Vine, "UK clinical guideline for the prevention and treatment of osteoporosis," *Archives of Osteoporosis*, vol. 12, pp. 1–43, 12 2017.

[2] C. Kim, M. C. Nevitt, J. Niu, M. M. Clancy, N. E. Lane, T. M. Link, S. Vlad, I. Tolstykh, P. M. Jungmann, D. T. Felson, and A. Guermazi, "Association of hip pain with radiographic evidence of hip osteoarthritis: diagnostic test study," *BMJ*, vol. 351, p. h5983, 12 2015.

[3] A. Woolf and B. Pfleger, "Burden of major musculoskeletal conditions. Bulletin of the World Health Organisation.," *Bulletin of the World Health Organization*, vol. 9, no. 03, p. 2003, 2003.

[4] J.-Y. Reginster and N. Burlet, "Osteoporosis: A still increasing prevalence," *Bone*, vol. 38, pp. 4–9, 2 2006.

[5] J. Damilakis, J. E. Adams, G. Guglielmi, and T. M. Link, "Radiation exposure in X-ray-based imaging techniques used in osteoporosis," 11 2010.

[6] S. P. Väänänen, *Functional Imaging of Proximal Femur by Combining Dual Energy X-ray Imaging and Finite Element Simulations*. PhD thesis, University of Eastern Finland, 2014.

[7] L. Grassi, *Femoral strength prediction using finite element models*. PhD thesis, Lund University, 2016.

[8] T. Heimann and H. P. Meinzer, "Statistical shape models for 3D medical image segmentation: A review," *Medical Image Analysis*, vol. 13, no. 4, pp. 543–563, 2009.

[9] L. H. Trammell and A. M. Kroman, "Bone and Dental Histology," in *Research Methods in Human Skeletal Biology*, pp. 361–395, Elsevier, 2013.

[10] J. Hanrahan and D. Horowitz, "Anatomy of a Joint," 2018.

[11] S. Kishner and T. R. Gest, "Hip Joint Anatomy," 2017.

[12] D.renard, "Pelvis," 2005. [Online; accessed February 9, 2018] https://commons.wikimedia.org/wiki/File:Pelvis.svg.

[13] S. Fidoe, "The hip bone," 2018. [Online; accessed February 8, 2018] http://teachmeanatomy.info/pelvis/bones/hip-bone/.

[14] N. Sarkalkan, H. Weinans, and A. A. Zadpoor, "Statistical shape and appearance models of bones," *Bone*, vol. 60, pp. 129–140, 2014.

[15] WebMD, 2016. [Online; accessed February 8, 2018] http://www.webmd.com/osteoarthritis/guide/hip-osteoarthritis-degenerative-arthritis-hip.

[16] M. Parker, "Hip fracture," *BMJ*, vol. 333, pp. 27–30, 7 2006.

[17] B. Ragnarsson and B. Jacobsson, "Epidemiology of pelvic fractures in a Swedish county.," *Acta orthopaedica Scandinavica*, vol. 63, no. 3, pp. 297–300, 1992.

[18] W. D. Bidgood, S. C. Horii, F. W. Prior, and D. E. Van Syckle, "Understanding and Using DICOM, the Data Interchange Standard for Biomedical Imaging," 1997.

[19] Y. Chen and G. Medioni, "Object modeling by registration of multiple range images," *Image and Vision Computing - Special issue: range image understanding*, vol. 10, no. 3, pp. 145–155, 1992.

[20] P. J. Besl and N. D. McKay, "A method for registration of 3-D shapes," *IEEE Transactions on Pattern Analysis and Machine Intelligence*, vol. 14, no. 2, pp. 239–256, 1992.

[21] F. Pomerleau, F. Colas, and R. Siegwart, "A Review of Point Cloud Registration Algorithms for Mobile Robotics," *Foundations and Trends in Robotics*, vol. 4, no. 1, pp. 1–104, 2015.

[22] Z. Zhang, "Iterative point matching for registration of free-form curves and surfaces," *International Journal of Computer Vision*, vol. 13, pp. 119–152, 10 1994.

[23] F. L. Bookstein, "Principal Warps: Thin-Plate Splines and the Decomposition of Deformations," *IEEE Transactions on Pattern Analysis and Machine Intelligence*, vol. 11, pp. 567–585, 6 1989.

[24] J. C. Gower, "Generalized procrustes analysis," *Psychometrika*, vol. 40, no. 1, pp. 33–51, 1975.

[25] I. T. Jolliffe and J. Cadima, "Principal component analysis: a review and recent developments," *Philosophical Transactions of the Royal Society A: Mathematical, Physical and Engineering Sciences*, vol. 374, p. 20150202, 4 2016.

[26] K. Pearson, "LIII. On lines and planes of closest fit to systems of points in space," *Philosophical Magazine Series 6*, vol. 2, pp. 559–572, 11 1901.

[27] H. Hotelling, "Analysis of a complex of statistical variables into Principal Components. Jour. Educ. Psych., 24, 417-441, 498-520," *The Journal of Educational Psychology*, vol. 24, pp. 417–441, 1933.

[28] Nicoguaro, "Gaussianscatterpca," 2016. [Online; accessed January 19, 2018].

[29] A. R. Syed, *A Review of Cross Validation and Adaptive Model Selection*. PhD thesis, Georgia State University, 2011.

[30] M. Viceconti and F. Taddei, "Automatic generation of finite element meshes from computed tomography data.," *Critical reviews in biomedical engineering*, vol. 31, no. 1-2, pp. 27–72, 2003.

[31] S. P. Väänänen, L. Grassi, G. Flivik, J. S. Jurvelin, and H. Isaksson, "Generation of 3D shape, density, cortical thickness and finite element mesh of proximal femur from a DXA image," *Medical Image Analysis*, vol. 24, pp. 125–134, 8 2015.

[32] MathWorks, 2017. MATLAB, Download from: https://se.mathworks.com/?s_tid=gn_logo.

[33] CIBC, 2016. Seg3D: Volumetric Image Segmentation and Visualization. Scientific Computing and Imaging Institute (SCI), Download from: http://www.seg3d.org.

[34] C. U. E. Department, 2017. Stradwin, Download from: http://mi.eng.cam.ac.uk/ rwp/stradwin/.

[35] G. M. Treece and A. H. Gee, "Independent measurement of femoral cortical thickness and cortical bone density using clinical CT," *Medical Image Analysis*, vol. 20, no. 1, pp. 249–264, 2015.

[36] A. HyperWorks, 2017. HyperMesh, Download from: https://altairhyperworks.com/Product/HyperMesh.

[37] D. Kroon, "Finite iterative closest point," 2009. [Online; accessed January 9, 2018].

[38] Manu, "nonrigidicp," 2017. [Online; accessed January 9, 2018].

[39] BodyParts3D, © The Database Center for Life Science licensed under CC Attribution-Share Alike 2.1 Japan., "Male right hip bone," 2012. [Online; accessed March 6, 2018] https://commons.wikimedia.org/wiki/File:Hip_bone_-_close-up_-_lateral_view_(right_hip_bone).png.

[40] H. Gray, *Anatomy of the Human Body*, vol. 157. Lea and Febiger, 20th ed., 1919.